J✈**M** PAPERS

The nonlinear evolution of internal tides. Part 1: the superharmonic cascade

Bruce R. Sutherland[1,2],† and Maninderpal S. Dhaliwal[1]

[1]Department of Physics, University of Alberta, Edmonton, Alberta T6G 2E1, Canada

[2]Department of Earth & Atmospheric Sciences, University of Alberta, Edmonton, Alberta T6G 2E3, Canada

In non-uniform stratification, horizontally propagating internal waves with the vertical structure of a single mode self-interact to excite superharmonics. Baker & Sutherland (*J. Fluid Mech.*, vol. 891, 2020, R1) showed that a vertical mode-1 parent wave of sufficiently small amplitude dominantly excites a vertical mode-1 superharmonic with double the horizontal wavenumber. Through theory, assuming a parent wave of sufficiently small amplitude, they showed that the superharmonics grew and decayed periodically due to the parent forcing frequency being off-resonant with the natural frequency of the superharmonic. Here, we extend this theory to allow for larger parent wave amplitudes and/or stronger resonant forcing, as would occur at lower latitudes, where the influence of background rotation is small. The resulting coupled system of nonlinear ordinary differential equations is shown to well predict the evolution of the internal tide as determined in fully nonlinear numerical simulations. With strong nonlinear forcing, successive superharmonics grow to non-negligible amplitudes in what we call the 'superharmonic cascade'. The phase relationship between the superharmonics is such that when superimposed, the internal tide transforms into a solitary wave train, consistent with the predictions of well-established shallow-water models, particularly that of the Ostrovsky equation, which is an extension of the Korteweg–de Vries equation accounting for background rotation. This work thus gives new insight into internal solitary wave generation. The model equations have less restrictive assumptions than models based upon shallow-water theory, and because they are quickly solved, these provide a potentially powerful new tool to examine the nonlinear evolution of the internal tide.

Key words: internal waves, waves in rotating fluids, solitary waves

† Email address for correspondence: bruce.sutherland@ualberta.ca

B.R. Sutherland and M.S. Dhaliwal

1. Introduction

Through its oscillatory motion across variable bottom topography, it is estimated that 1 TW of the power of the barotropic tide is converted into internal (baroclinic) tides (Wunsch & Ferrari 2004). The internal tides consequently transmit energy throughout the oceans until the energy is converted to smaller and smaller scales, ultimately resulting in turbulent mixing (MacKinnon *et al.* 2017). At its generation site, the oscillation of the barotropic tide over sufficiently steep submarine topography launches vertically propagating beams (Balmforth, Ierley & Young 2002; Legg & Adcroft 2003). After these beams interact with the near-surface stratification, they are observed to transform into horizontally propagating low-vertical-mode disturbances, dominated primarily by the lowest (mode-1) disturbance. In some regions, notably the South China Sea, the internal tide is observed to transform into a relatively large amplitude train of internal solitary waves (Alford *et al.* 2010; Li & Farmer 2011). In other locations, the waves are observed to propagate long distances without any such transformation (Alford 2003; Alford *et al.* 2007; MacKinnon *et al.* 2013; Klymak *et al.* 2016). The work presented here examines what influences the nonlinear steepening of the internal tide, focusing upon the initial amplitude of the vertical mode-1 internal tide and the latitude at which it propagates. We will show that the potential for steepening is enhanced as the influence of the Coriolis force lessens (near the equator), and that this steepening can be seen to result from the sequential excitation of mode-1 disturbances having progressively higher superharmonic horizontal wavenumbers.

Inspired by observations of the apparent localized generation of solitary waves in the central Bay of Biscay (New & Pingree 1990, 1992), laboratory and numerical studies showed that successive superharmonics can be excited by an upward-propagating internal wave beam incident upon a pycnocline (Grisouard, Staquet & Gerkema 2011; Wunsch & Brandt 2012; Diamessis *et al.* 2014).

More recent studies have shown that even in the absence of vertically propagating internal wave beams, horizontally propagating two-dimensional (spanwise-invariant) internal modes self-interact to excite superharmonics provided that the background stratification is non-uniform (Sutherland 2016; Wunsch 2017; Baker & Sutherland 2020). Most of these studies focused upon the steady state co-existence between the internal tide (which we refer to here as the 'parent wave') having horizontal wavenumber k, and its superharmonic with double the horizontal wavenumber, $2k$. By 'steady state', it is meant that the amplitudes of the parent and superharmonic waves are constant in time. However, Baker & Sutherland (2020) showed that ultimately, such a steady state does not evolve from a horizontally periodic internal mode: starting with no superharmonics, the parent wave excites internal waves that grow and decay periodically in amplitude, provided that the amplitude of the parent wave is sufficiently small. In our companion paper (Sutherland & Yassin 2022), we likewise show that ultimately, a steady state does not evolve from horizontally modulated internal modes. This occurs because the natural frequency, ω_2, of the superharmonic wave is nearly double the frequency, ω, of the parent wave. The mismatch between the ω_2 and 2ω frequencies initially leads to the constructive growth of the superharmonic followed by its destructive decay. The resulting beat frequency of the superharmonics is set by the degree of mismatch between the frequencies, as represented by the non-dimensional parameter $\epsilon = ((2\omega)^2 - \omega_2^2)/(2\omega)^2$. Because this parameter is small, the self-interaction of a vertical mode-1 parent wave excites a nearly pure vertical mode-1 superharmonic disturbance.

In the study by Baker & Sutherland (2020), the beat frequency of the $2k$-superharmonic was predicted to be $\epsilon\omega$, and the maximum amplitude of the superharmonic relative to

the amplitude parent wave was set by the ratio α/ϵ, in which α is the ratio of the initial maximum vertical displacement of the parent wave to the characteristic depth of the stratification. That study, which focused exclusively on the interactions between the parent and the $2k$-superharmonic alone, was shown to be accurate provided that $\alpha/\epsilon \ll 1$. For larger α/ϵ, the growth of higher superharmonics cannot be ignored. The main theoretical advance of this paper is to relax the restriction that α/ϵ is small, and so consider interactions between the parent wave and an arbitrary number of its superharmonics.

It is certainly possible for internal tides in the ocean to have sufficiently large amplitude such that $\alpha/\epsilon \gtrsim 1$. This is particularly true for internal tides near the equator, in which case $\omega_2 \simeq 2\omega$ (and $\epsilon \ll 1$) because the dispersion relation relating ω to k is approximately linear for long waves ($kH \ll 1$, with H being the ocean depth) if the Coriolis parameter is zero. For this reason, the parameter regime of our study is motivated by observations of the internal tide that emanates south-west of Hawaii towards the equator.

In § 2 we review the far-field observations of the internal tide south-west of Hawaii. These are used to motivate the parameter regimes explored in our study. We then present, in § 3, the theory leading to a coupled system of nonlinear ordinary differential equations describing the growth (and possible decay) of successive superharmonics. Solutions as they depend upon the parent wave amplitude and latitude of propagation are given therein. Section 4 describes the fully nonlinear code used to simulate the evolution of the internal tide. Therein it is shown that the predictions in § 3 well represent the fully nonlinear results. Observing that the model predicts that the internal tide transforms into an internal solitary wave train if α/ϵ is large, § 5 reviews models based on shallow-water theory that likewise produce solitary wave trains. Their predictions are then compared to our model. Discussion and conclusions are presented in § 6.

2. Parameter regime

For the parameters explored in this study, we focus on the 'Farfield' observations of the internal tide that propagated south-west of the Hawaiian Islands (Rainville & Pinkel 2006). These observations, taken over 40 days in the autumn of 2001, were made 430 km south-west of Oahu at a latitude of 18.39°N. The Coriolis parameter at that latitude was 0.0000459 s^{-1}, in which here, and throughout this paper, we write s^{-1} to represent radians per second. The ocean depth at the Farfield location was $H \simeq 5200$ m.

Measurements of temperature and conductivity (salinity) taken between the surface and 800 m depth showed that the background density profile decreased approximately exponentially with depth below a 100 m deep surface mixed layer. In particular, the buoyancy frequencies at 100 m and 800 m depth were approximately 10 and 2 cycles per hour (c.p.h.), respectively. From these data, we estimate the background squared buoyancy frequency profile below $z_0 = -100$ m to be $N^2(z) \simeq N_0^2\, e^{(z-z_0)/d}$, with $N_0 \simeq 0.017$ s^{-1} ($\simeq 9.7$ c.p.h.) and $d \simeq 218$ m.

From measurements of both the isopycnal displacements and baroclinic energy flux, the dominant disturbances to the background took the form of vertical mode-1 internal tides at the semi-diurnal frequency of the lunar (M_2) tide, $\omega \simeq 0.000141$ s^{-1}. Satellite altimetry and numerical modelling determined the horizontal wavelength of the M_2 internal tide to be approximately 150 km (Rainville *et al.* 2010). The corresponding horizontal wavenumber is $k \simeq 4.2 \times 10^{-5}$ m^{-1}.

The root-mean-square isopycnal displacements of the semi-diurnal tide was largest between 400 and 700 m depth, with values $\gtrsim 25$ m at the spring tides, and $\lesssim 5$ m at

the neap tides (Rainville & Pinkel 2006). From this we estimate the half peak-to-peak displacement to be $A_0 \simeq 15 \ (\pm 10)$ m.

We use these data to cast the key variables of our study as non-dimensional parameters that will guide approximations used in the following theory section as well as setting variables used in numerical simulations. The e-folding depth of the stratification relative to the ocean depth is $d/H \simeq 0.04$. The relative Coriolis and internal tide frequencies are $f/N_0 \simeq 0.003$ and $\omega/N_0 \simeq 0.008$, respectively. The relative horizontal wavenumber is $kH \simeq 0.2$. The half peak-to-peak amplitude relative to the ocean depth is $A_0/H \simeq 0.003 \ (\pm 0.002)$. Taken relative to the e-folding depth of the stratification, we have $\alpha \equiv A_0/d \simeq 0.075 (\pm 0.050)$.

We are particularly interested in the behaviour of the internal tide as it travels south towards the equator, where $f = 0$. Thus we neglect variations in bottom depth and assume that $kH \simeq 0.2$ is fixed. For simplicity, the equations are solved on the f-plane, with the evolution of the internal tide examined separately at different fixed values of f between $0.003 N_0$ and 0.

3. Theory

Here, we present the theory for superharmonic excitation induced by a horizontally propagating, vertical mode-1 internal wave. After presenting the equations of motion, the vertical structure equation and polarization relations for small-amplitude internal waves are presented. Evolution equations are then derived for superharmonics excited by triad interactions between internal modes. In this work, we ignore the self-interaction of waves leading to an induced Eulerian flow (Bühler 2014; van den Bremer, Yassin & Sutherland 2019). This is because, as is shown in our companion paper (Sutherland & Yassin 2022), superharmonics are near-resonant with the parent wave, whereas the induced Eulerian flow is not. Hence this flow has negligible influence upon the parent wave and its superharmonics.

3.1. *Equations of motion*

We consider the motion of inviscid, non-diffusive, incompressible Boussinesq fluid on the f-plane in a horizontally periodic channel bounded above and below by free-slip boundary conditions. The waves in this domain are taken to be two-dimensional, having structure in the along-wave (x) and vertical (z) directions. Although there can be motion in the spanwise (y) direction, the fields of interest are independent of y.

The momentum equations are

$$\frac{Du}{Dt} - fv = -\frac{1}{\rho_0}\frac{\partial p}{\partial x}, \quad \frac{Dv}{Dt} + fu = 0, \quad \frac{Dw}{Dt} = -\frac{1}{\rho_0}\frac{\partial p}{\partial z} + b, \quad (3.1a\text{--}c)$$

in which $D/Dt \equiv \partial_t + u\partial_x + w\partial_z$ is the material derivative, u, v and w are the components of velocity in the x, y and z directions, respectively, $b = -g\rho/\rho_0$ is the buoyancy, p and ρ are the pressure and density fluctuations, respectively, and ρ_0 is the characteristic density. In these expressions, gravity (g) and the Coriolis parameter (f) are assumed to be constant. From internal energy conservation, we have

$$\frac{Db}{Dt} = -N^2 w, \quad (3.2)$$

in which $N^2(z) = -(g/\rho_0)\,d\bar{\rho}/dz$ is the squared buoyancy frequency, and $\bar{\rho}(z)$ is the background density. In a uniformly stratified fluid, $\bar{\rho}$ increases linearly with depth and N^2

is constant. In this study, N^2 is taken to be z-dependent, as is necessary for the excitation of superharmonics.

By assuming that the fluid is incompressible, the x- and z-velocity components can be written in terms of the streamfunction ψ:

$$u = -\frac{\partial \psi}{\partial z}, \quad w = \frac{\partial \psi}{\partial x}. \tag{3.3a,b}$$

Taking the curl of the x- and z-momentum equations gives an equation for the evolution of the spanwise vorticity, $\zeta \equiv \partial_z u - \partial_x w$:

$$\frac{\mathrm{D}\zeta}{\mathrm{D}t} = -\frac{\partial b}{\partial x} + f\frac{\partial v}{\partial z}. \tag{3.4}$$

These nonlinear equations can be manipulated to be written as a linear operator acting on the streamfunction ψ, being forced by nonlinear terms (Wunsch 2017; Baker & Sutherland 2020):

$$\mathcal{L}\psi = \nabla \cdot \boldsymbol{F}, \tag{3.5}$$

in which

$$\mathcal{L} \equiv \partial_{tt}\nabla^2 + N^2\partial_{xx} + f^2\partial_{zz} \tag{3.6}$$

and

$$\boldsymbol{F} \equiv \partial_t(\boldsymbol{u}\zeta) - \partial_x(\boldsymbol{u}b) + f\,\partial_z(\boldsymbol{u}v). \tag{3.7}$$

Here, $\nabla^2 = \partial_{xx} + \partial_{zz}$ is the Laplacian, and t, x and z subscripts denote the corresponding partial derivatives. In solving the above equations, the domain is taken to be bounded above and below by free-slip horizontal boundaries at $z = 0$ and $z = -H$.

3.2. *Small-amplitude waves*

Laying the groundwork for the nonlinear studies that follow, here we describe the initial structure of the internal tide, which we refer to hereafter as the 'parent wave', and then generalize this to describe the structure and polarization relations associated with the parent wave and its superharmonics.

The parent wave has a prescribed horizontal wavenumber k, and vertical displacement amplitude A_0. Although in reality the internal tide is modulated spatially, it is unnecessary to include these dynamics in the consideration of superharmonic excitation. The streamfunction characterizing the parent wave is given by

$$\psi^{(1)} = \frac{1}{2}\frac{\omega d}{k}\,\alpha\,a_1(T)\,\hat{\psi}_1(z)\,\mathrm{e}^{\mathrm{i}(kx-\omega t)} + \mathrm{c.c.}, \tag{3.8}$$

in which c.c. denotes the complex conjugate, and $a_1(T)$ represents the slow time (T) evolution of amplitude, to be discussed in detail below. Somewhat arbitrarily, we have introduced d to be the characteristic vertical scale of variation of $N^2(z)$, so that $\alpha \equiv A_0/d$ is the non-dimensional initial amplitude of the parent wave, expressed as the maximum vertical displacement relative to d. Substituting (3.8) into $\mathcal{L}\psi^{(1)} = 0$ gives an eigenvalue problem for the vertical structure $\hat{\psi}_1$ and its associated frequency ω:

$$\hat{\psi}_1'' + k^2\frac{N^2 - \omega^2}{\omega^2 - f^2}\,\hat{\psi}_1 = 0, \quad \hat{\psi}_1(-H) = \hat{\psi}_1(0) = 0. \tag{3.9}$$

As justified below (see also Baker & Sutherland 2020), we consider only superharmonics having the vertical structure of mode-1 waves for which $\hat{\psi}_1(z) > 0$ for $-H < z < 0$.
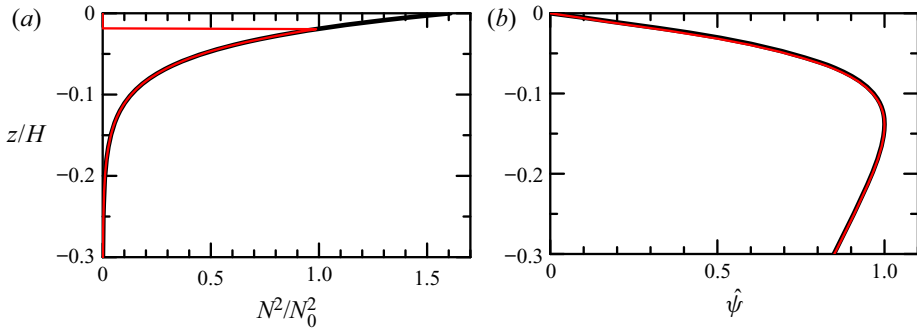
Figure 1. (*a*) Profiles of exponential stratification with $d = 0.04H$ and $N = N_0$ at $z_0 = -0.019H$ (thick black line) and of the same exponential stratification but with $N = 0$ above $z = -0.019H$ (red line). (*b*) The corresponding vertical structure functions of mode-1 waves. The structure was computed for $k = 0.2H$ and $f = 0.003N_0$. In both cases, only the top 30 % of the full domain height is plotted.

These eigenfunctions are normalized so that $\max\{\hat{\psi}_1\} = 1$. The vertical structure is plotted in figure 1 as computed for waves in exponential stratification,

$$N^2(z) = N_0^2 \, e^{(z-z_0)/d} \quad \text{for } -H \leq z \leq 0, \tag{3.10}$$

and in exponential stratification that includes a surface mixed layer

$$N^2(z) = \begin{cases} 0 & z_0 < z \leq 0, \\ N_0^2 \, e^{(z-z_0)/d} & -H \leq z \leq z_0. \end{cases} \tag{3.11}$$

In both cases, we set $d = 0.04H$ and $z_0 = -0.019H$, equivalent to a 100 m deep mixed layer in an ocean of depth $H = 5200$ m. These plots demonstrate that the vertical structure is not particularly sensitive to the presence of a mixed layer. The peak in the vertical structure occurs at depth $-0.14H$ (approximately 700 m depth), which is comparable to the maximum isopycnal displacements observed at the Farfield site south-west of Hawaii (Rainville & Pinkel 2006).

The evolution of the parent wave is given by $a_1(T)$, in which $T = \epsilon t$ describes the slow time variation ($\epsilon \ll 1$) of the parent wave due to interactions with the superharmonics that it excites. With the streamfunction defined by (3.8), the initial non-dimensional amplitude of the parent wave is $a_1(0) = 1$. As in Baker & Sutherland (2020), we will show that the small parameter ϵ is determined by the degree to which the forcing of the $2k$-superharmonic by the parent wave at frequency 2ω is off-resonant with the natural frequency ω_2 of the mode-1 superharmonic.

The parent wave self-interacts through the nonlinear terms in (3.7) to excite a superharmonic with wavenumber $2k$. The parent wave and its $2k$-superharmonic can then interact creating higher superharmonics, modifying the amplitude of the parent wave and superharmonics in time.

For convenience, we write the streamfunction for each of the parent ($n = 1$) and its superharmonics ($n = 2, 3, \ldots$) as

$$\psi^{(n)} = \frac{1}{2} \alpha \, \frac{\omega d}{k} \, \psi_n \, e^{in(kx-\omega t)} + \text{c.c.}, \tag{3.12}$$

in which

$$\psi_n = a_n(T) \, \hat{\psi}_n(z), \quad n = 1, 2, 3, \ldots . \tag{3.13}$$

Field	Polarization relation
ψ_n	$a_n \hat{\psi}_n$
u_n	$-a_n \hat{\psi}'_n$
v_n	$i\,\frac{f}{n\omega}\,a_n \hat{\psi}'_n$
w_n	$inka_n \hat{\psi}_n$
b_n	$N^2\,\frac{k}{\omega}\,a_n \hat{\psi}_n$
ζ_n	$\frac{k^2}{\omega^2}\,\frac{N^2-f^2}{\omega_n^2-f^2}\,\omega_n^2 a_n \hat{\psi}_n$

Table 1. Expressions for the polarization relations of the fields with horizontal wavenumber nk, $n = 1, 2, \ldots$. The actual fields are found by multiplying by $\alpha(\omega d/k)\,\exp[in(kx - \omega t)]/2$ and adding the complex conjugate. In these expressions, primes on $\hat{\psi}_n$ denote z-derivatives.

The vertical structure is given by the solution to the eigenvalue problem

$$\hat{\psi}''_n + (nk)^2\,\frac{N^2 - \omega_n^2}{\omega_n^2 - f^2}\,\hat{\psi}_n = 0, \quad \hat{\psi}_n(-H) = \hat{\psi}_n(0) = 0, \quad n = 1, 2, 3, \ldots, \quad (3.14)$$

in which ω_n is the natural frequency of a vertical mode-1 wave having wavenumber nk. As in (3.8), the amplitude $a_n(T)$ of the waves is assumed to depend upon a slow time scale $T = \epsilon t$.

The expression for $\psi^{(n)}$ supposes that the frequency of the wave with wavenumber nk is $n\omega$. This assumption is made because integer multiples of the parent wave frequency result from wave–wave interactions in the nonlinear terms. However, for $n > 1$, the frequency $n\omega$ is not equal to the natural frequency ω_n of the mode-1 wave with wavenumber nk, although the difference in frequencies may be close, as demonstrated in the next subsection. It is this slight mismatch that leads to off-resonant forcing of successive superharmonics.

Given the streamfunction of the parent wave and its superharmonics, the other fields appearing in the nonlinear terms of F in (3.7) can be found from the polarization relations. These expressions are listed in table 1.

3.3. Superharmonic cascade

Now consider the triad interaction in which a wave having wavenumber lk interacts with a wave having wavenumber mk to force a disturbance with wavenumber nk, in which $n = l + m$. Here, l, m and n can be negative as well as positive integers, with negative numbers arising from the complex conjugate terms in the polarization relations. From (3.7), the nonlinear forcing of nk-waves by mk- and lk-waves is given by

$$\nabla \cdot F_{ml} = \nabla \cdot [\partial_t(u_m \zeta_l) - \partial_x(u_m b_l) + f\,\partial_z(u_m v_l)], \quad |m|, |l| \geq 1, \quad (3.15)$$

in which $n = m + l$.

To find the response to the forcing, we use (3.6) to expand $\mathcal{L}\psi^{(n)}$, with time derivatives acting upon $a_n(T)$ as well as the complex exponential. However, assuming that ϵ is small,

the term $\epsilon^2 \, \mathrm{d}^2 a_n / \mathrm{d}T^2$ can be neglected. Thus we find, for $n = 1, 2, 3, \ldots$,

$$\mathcal{L}\psi^{(n)} \simeq \frac{1}{2} \, \alpha \, \frac{\omega d}{k} \, (nk)^2 \, \frac{N^2 - f^2}{\omega_n^2 - f^2} \left[2\mathrm{i}n\omega\epsilon \, \frac{\mathrm{d}a_n}{\mathrm{d}T} + [(n\omega)^2 - \omega_n^2]a_n \right] \hat{\psi}_n \, \mathrm{e}^{\mathrm{i}n(kx - \omega t)}. \quad (3.16)$$

As in Baker & Sutherland (2020), we recognize that $\omega_2 \simeq 2\omega$, and so define the slow time evolution parameter ϵ to be

$$\epsilon \equiv \frac{4\omega^2 - \omega_2^2}{4\omega^2}. \quad (3.17)$$

For convenience, we make the following definition:

$$B_1 = 0, \quad B_n = \frac{2}{n(n-1)} \frac{n^2\omega^2 - \omega_n^2}{4\omega^2 - \omega_2^2}, \quad n = 2, 3, \ldots. \quad (3.18a,b)$$

In particular, $B_2 = 1$ and empirical calculations show that $B_n \sim 1$ for sufficiently small $n \geq 2$ and f/N_0 not negligibly small. Explicit approximate analytical expressions for B_n are given in Appendix A.

With these definitions, (3.16) becomes

$$\mathcal{L}\psi^{(n)} \simeq \alpha \, \frac{\omega d}{k} \, (\mathrm{i}n^3 k^2 \omega\epsilon) \frac{N^2 - f^2}{\omega_n^2 - f^2} \left[\frac{\mathrm{d}a_n}{\mathrm{d}T} - \mathrm{i}(n-1)\omega B_n a_n \right] \hat{\psi}_n \, \mathrm{e}^{\mathrm{i}n(kx - \omega t)}. \quad (3.19)$$

Equating (3.15) and (3.19), we get the following equation for the forcing of waves having wavenumber nk:

$$\left[\frac{\mathrm{d}a_n}{\mathrm{d}T} - \mathrm{i}(n-1)\omega B_n a_n \right] (N^2 - f^2)\hat{\psi}_n = -\frac{\mathrm{i}}{\epsilon} \frac{\omega_n^2 - f^2}{n^3 k \omega^2 d} \, \mathrm{e}^{-\mathrm{i}n(kx - \omega t)} \, \alpha^{-1} \sum_{m+l=n} \nabla \cdot \boldsymbol{F}_{ml}. \quad (3.20)$$

In the sum, $n \geq 1$, $m \geq l$, and both m and l are non-zero integers, since here we are neglecting the generation of and interactions with the induced Eulerian flow. By construction, the complex exponentials in front of and (implicitly) within the sum cancel out.

While the vertical structure of the forcing on the right-hand side can be seen as a superposition of vertical modes, the response to this forcing is dominantly a mode-1 disturbance (Baker & Sutherland 2020). The forcing of the mode-1 wave is found using the orthogonality of modes under the weight $N^2 - f^2$. Thus multiplying both sides of (3.20) by $\hat{\psi}_n$ and integrating in z from $-H$ to 0 gives the ordinary differential equation governing the time evolution of $a_n(T)$. The result is a hierarchy of equations written explicitly in terms of the amplitude functions a_n:

$$\frac{\mathrm{d}a_n}{\mathrm{d}T} - \mathrm{i}(n-1)\omega B_n a_n = -\mathrm{i}\alpha \, \frac{\omega}{\epsilon} \sum_{m+l=n, m \geq l} E_{ml} a_m a_l, \quad n = 1, 2, 3, \ldots, \quad (3.21)$$

in which l is non-zero and $a_{-l} = a_l^\star$, the complex conjugate of a_l. The coefficients E_{ml} are real and positive constants. Explicitly, for $m = l$ (and $n = 2m$) these are

$$E_{mm} = \frac{1}{8n} \, d \, \frac{\omega_n^2 - f^2}{\omega^2} \left[\int_{-H}^0 (N^2 - f^2)\hat{\psi}_n^2 \, \mathrm{d}z \right]^{-1}$$

$$\times \left\{ \left(1 + \frac{1}{2} \frac{nm\omega^2 + f^2}{\omega_m^2 - f^2} \right) \int_{-H}^0 \frac{\mathrm{d}N^2}{\mathrm{d}z} \hat{\psi}_m^2 \hat{\psi}_n \, \mathrm{d}z \right\}, \quad (3.22)$$

and for $m > l$ (and $n = m + l$),

$$
E_{ml} = \frac{1}{4n} \, d \, \frac{\omega_n^2 - f^2}{\omega^2} \left[\int_{-H}^{0} (N^2 - f^2) \hat{\psi}_n^2 \, \mathrm{d}z \right]^{-1}
$$

$$
\times \left\{ \left[1 + \frac{ml}{n^2} \left(\frac{nl\omega^2 + f^2}{\omega_l^2 - f^2} + \frac{nm\omega^2 + f^2}{\omega_m^2 - f^2} \right) \right] \int_{-H}^{0} \frac{\mathrm{d}N^2}{\mathrm{d}z} \hat{\psi}_m \hat{\psi}_l \hat{\psi}_n \, \mathrm{d}z \right.
$$

$$
+ \frac{\omega^2}{n} \left(\frac{m^2}{\omega_m^2 - f^2} - \frac{l^2}{\omega_l^2 - f^2} \right) \int_{-H}^{0} (N^2 - f^2)(l\hat{\psi}_m' \hat{\psi}_l \hat{\psi}_n - m\hat{\psi}_m \hat{\psi}_l' \hat{\psi}_n) \, \mathrm{d}z
$$

$$
+ f^2 \frac{1}{n^2} \int_{-H}^{0} l(m - 2l) \frac{N^2 - \omega_l^2}{\omega_l^2 - f^2} \hat{\psi}_m' \hat{\psi}_l \hat{\psi}_n + m(l - 2m) \frac{N^2 - \omega_m^2}{\omega_m^2 - f^2} \hat{\psi}_m \hat{\psi}_l' \hat{\psi}_n \, \mathrm{d}z
$$

$$
\left. + f^2 \frac{ml}{n^2} \int_{-H}^{0} \frac{N^2 - \omega_l^2}{\omega_l^2 - f^2} \hat{\psi}_m \hat{\psi}_l' \hat{\psi}_n + \frac{N^2 - \omega_m^2}{\omega_m^2 - f^2} \hat{\psi}_m' \hat{\psi}_l \hat{\psi}_n \, \mathrm{d}z \right\}, \tag{3.23}
$$

in which $\omega_{-l} = \omega_l$ and $\hat{\psi}_{-l} = \hat{\psi}_l$.

The expressions for the interaction coefficients simplify significantly if we assume that the primary wave and the most significant excited superharmonics ($n \le n_\star$) can all be treated as long waves, with $(n_\star k)H \ll 1$. Their derivations are given in Appendix A. In particular, this analysis shows that, independent of f, the dominant contribution to E_{ml} comes from the term involving $\mathrm{d}N^2/\mathrm{d}z$, and that $E_{ml} \simeq 2E_{jj}$ if $m > l$ and $m + l = 2j$.

Table 2 lists values of these coefficients as they depend upon the characteristic wavenumber of the internal tide, the e-folding depth of the stratification and the relative Coriolis parameter. The coefficients E_{ml} change little with the variations in kH, d/H and f/N_0, which is consistent with the long-wave approximations (A2) and (A3). The most significant changes occur for ϵ, which decreases rapidly as f/N_0 goes to zero. Consistent with (A7), the coefficient B_3 is close to 8/9 for sufficiently large f, but $B_3 \simeq 2$ if $f = 0$.

The coefficients ϵ, B_n and E_{ml} were also computed for stratification having a surface mixed layer given approximately by (3.11), though to avoid the singularity in $\mathrm{d}N^2/\mathrm{d}z$, a hyperbolic tangent function was used to connect the uniform-density layer to the exponential stratification over a distance $0.1z_0$. The values were found to differ by less than 3 % of the values in the table, consistent with a surface mixed layer having little effect upon the vertical structure function, as shown in figure 1. The coefficients were more sensitive to changing the stratification at depth by weakening the exponential decay at depth of the buoyancy frequency to be more representative of that in the abyss. A detailed exploration of the influence of the structure of the stratification upon the interaction coefficients goes beyond the scope of our present study.

In the special case of the self-interaction of the parent, as determined by the coupling coefficient E_{11}, (3.22) shows that this leads to superharmonics only if the fluid is non-uniformly stratified, as has been noted previously (Wunsch 2015, 2017; Sutherland 2016; Varma & Mathur 2017; Baker & Sutherland 2020).

Baker & Sutherland (2020) examined the truncated system of equations involving only the parent self-interaction creating a $2k$-superharmonic, and the $2k$-superharmonic interacting with the parent so as to modify the parent. Respectively, these are given explicitly by

$$
\frac{\mathrm{d}a_2}{\mathrm{d}T} - \mathrm{i}\omega a_2 = -\mathrm{i}\alpha \frac{\omega}{\epsilon} E_{11} a_1^2, \quad \frac{\mathrm{d}a_1}{\mathrm{d}T} = -\mathrm{i}\alpha \frac{\omega}{\epsilon} E_{2,-1} a_2 a_1^\star. \tag{3.24a,b}
$$

948 A21-9

kH	d/H	f/N_0	ϵ	B_3	$E_{2,-1}$	$E_{3,-2}$	$E_{1,1}$	$E_{3,-1}$	$E_{2,1}$
0.1	0.04	0.010	0.65	0.89	0.31	0.33	0.31	0.46	0.79
0.1	0.04	0.004	0.38	0.89	0.34	0.35	0.34	0.60	0.95
0.1	0.04	0.003	0.27	0.89	0.36	0.36	0.36	0.65	1.01
0.1	0.04	0.002	0.15	0.89	0.37	0.38	0.37	0.71	1.08
0.1	0.04	0.001	0.045	0.91	0.39	0.39	0.38	0.76	1.14
0.1	0.04	0	0.0009	1.99	0.39	0.39	0.39	0.78	1.17
0.2	0.04	0.010	0.46	0.89	0.33	0.35	0.33	0.56	0.89
0.2	0.04	0.004	0.15	0.91	0.37	0.38	0.37	0.71	1.07
0.2	0.04	0.003	0.096	0.92	0.38	0.38	0.38	0.74	1.10
0.2	0.04	0.002	0.047	0.96	0.39	0.39	0.38	0.76	1.13
0.2	0.04	0.001	0.015	1.14	0.39	0.39	0.39	0.78	1.15
0.2	0.04	0	0.0035	1.97	0.39	0.39	0.39	0.78	1.16
0.2	0.08	0.010	0.27	0.90	0.37	0.38	0.37	0.67	1.03
0.2	0.08	0.004	0.067	0.98	0.40	0.40	0.39	0.77	1.15
0.2	0.08	0.003	0.041	1.04	0.40	0.40	0.40	0.79	1.17
0.2	0.08	0.002	0.022	1.17	0.40	0.40	0.40	0.80	1.18
0.2	0.08	0.001	0.010	1.52	0.40	0.41	0.40	0.80	1.19
0.2	0.08	0	0.006	1.96	0.40	0.41	0.40	0.81	1.19

Table 2. Non-dimensional coefficients used to compute the evolution of the parent wave with horizontal wavenumber k and its first two superharmonics, $2k$ and $3k$ ($n_\star = 3$). The background N^2 profile is exponential, given by (3.10). In all cases, $z_0 = -0.019H$ and the e-folding depth of the stratification is $d = 0.04H$ or $0.08H$, as indicated. The Coriolis parameter, given relative to $N_0 \simeq 0.017 \text{ s}^{-1}$, ranges from values near Hawaii to $f = 0$ at the equator as well as the case $f/N_0 = 0.01$.

If the parent wave amplitude is sufficiently small, then the influence of the superharmonic upon the parent can be neglected, in which case $a_1(T) = 1$, and the first equation gives $a_2(T) = E_{11}(\alpha/\epsilon)[1 - \exp(\mathrm{i}\omega T)]$. Recalling that $T = \epsilon t$, this shows that the superharmonic grows and decays periodically with frequency $\epsilon\omega$. Also, the $2k$-superharmonic grows to amplitude $\propto \alpha/\epsilon$ with respect to the parent. So the truncation of equations leading to (3.24a,b) is valid provided that $\alpha/\epsilon \ll 1$ (Baker & Sutherland 2020).

If $\alpha/\epsilon \gtrsim 1$, then the $2k$-superharmonic can grow to non-negligible amplitude with respect to the parent. If the relative amplitude is fixed, but α/ϵ is large due to ϵ being small, then the $2k$-superharmonic would remain large for longer times owing to the smaller beat frequency $\epsilon\omega$. Thus, in this circumstance, it is anticipated that the parent and $2k$-superharmonic should excite higher superharmonics.

Such considerations are not just a theoretical exercise. Although realistic internal tides have small amplitude, circumstances can exist where $\alpha/\epsilon \gg 1$ as a consequence of ϵ being smaller than α. This is particularly likely near the equator where the cut-off frequency f in the dispersion relation goes to zero so that, approaching the limit of very long waves ($kH \to 0$), $\omega \propto k$. Hence $2\omega(k) = \omega_2 \equiv \omega(2k)$, in which case $\epsilon = 0$. This is illustrated in figure 2, for which the dispersion relation is computed for mode-1 waves in exponential stratification with e-folding depth $d = 0.04H$. At latitudes where $f/N_0 = 0.008$, ω_2 is moderately offset from 2ω so that $\epsilon \simeq 0.18$ for $kH = 0.2$. However, at the equator there is near perfect resonance between the parent mode forcing frequency at 2ω and the natural frequency of the $2k$-superharmonic, as indicated by the low value of $\epsilon \simeq 0.007$. Even for a parent tide with a relatively small vertical displacement amplitude $A_0 = 5$ m in an ocean of depth $H \simeq 5$ km and stratification with e-folding depth $d \simeq 200$ m, the non-dimensional
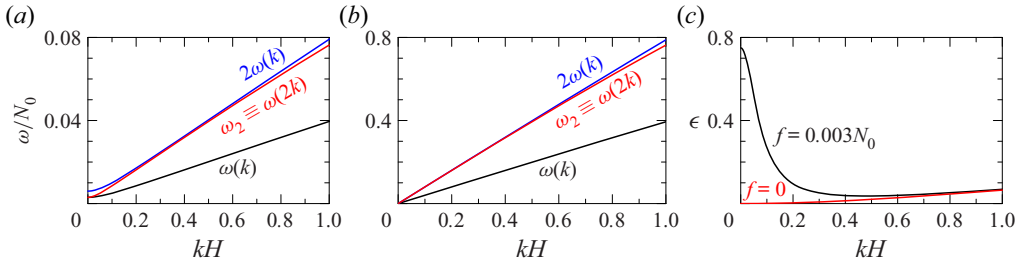
Figure 2. For mode-1 waves in stratification given by (3.10) with $d = 0.04H$ and $z_0 = -0.019H$, plots of the dispersion relation and comparison of 2ω with ω_2, with (a) $f = 0.003N_0$, and (b) $f = 0$. Plots of the corresponding values of ϵ are shown in (c) for $f = 0.003N_0$ and $f = 0$.
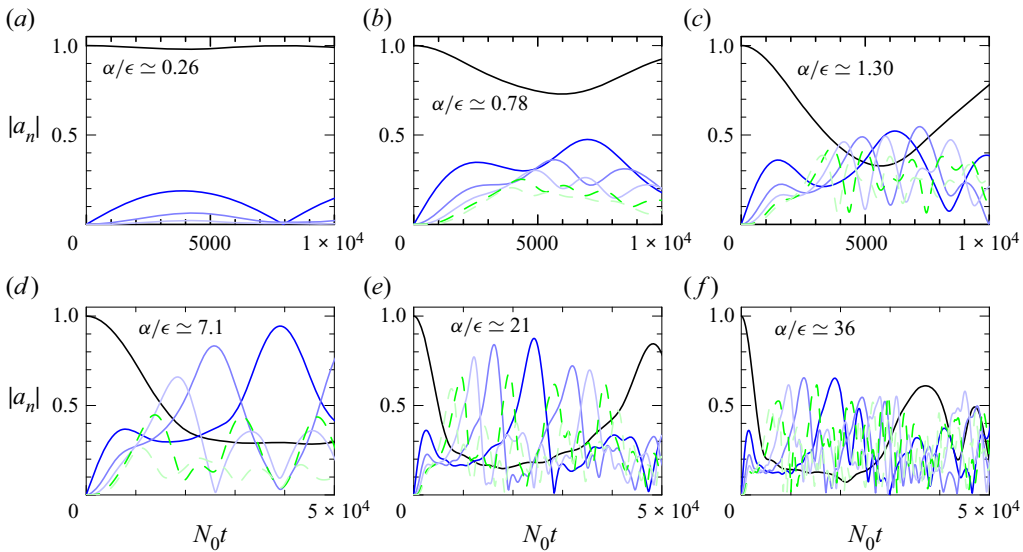

Figure 3. Time evolution of the amplitudes a_n, shown for the parent ($n = 1$, solid black lines) and the first five superharmonics ($n = 2$, dark blue; $n = 3$, medium blue; $n = 4$, light blue; $n = 5$, dashed green; $n = 6$, dashed pale green), computed for (a–c) $f = 0.003N_0$ ($\epsilon \simeq 0.096$), and (d–f) $f = 0$, ($\epsilon \simeq 0.0035$), and for amplitudes (a,d) $\alpha = 0.025$, (b,e) $\alpha = 0.075$, and (c,f) $\alpha = 0.125$. In all cases, $k = 0.2H$ and the background stratification is exponential with $N = N_0$ at $z_0 = -0.019H$ and $d = 0.04H$, and the solutions of (3.21) were found by setting a truncation level of $n_\star = 20$.

amplitude $\alpha \simeq A_0/d = 0.025$ is larger than ϵ. This implies that progressively higher superharmonics may be excited as internal tides approach the equator.

For given stratification, Coriolis parameter and parent wave horizontal wavenumber, the coefficients in (3.21) can be evaluated up to some truncation level $n \leq n_\star$. There are then $n_\star$ coupled equations involving terms with both $m \leq n_\star$ and $|l| < n_\star$. For $\alpha/\epsilon \ll 1$, it is sufficient to choose $n_\star = 2$, leading to the pair of equations given by (3.24a,b). For the studies below of the internal tide approaching the equator, α/ϵ can be much larger than 1. In these cases, convergence of solutions is found by including superharmonics up to $n_\star = 20$.

The system of ordinary differential equations was solved by straightforward time integration with equally spaced time steps ΔT. With $\Delta T = 0.001$ and $n_\star = 20$, MATLAB integrated the equations over the time of one beat period $2\pi/(\epsilon\omega)$ in $\simeq 10$ s of real time

on a single 2.7 GHz core. After the solutions were found, the results were rescaled to time $t = T/\epsilon$. The results are shown in figure 3 for cases in which the Coriolis parameter is representative of that near Hawaii and at the equator. Amplitudes are based upon observations of the tide between the neap and spring cycles.

For the smallest amplitude case with $f = 0.003N_0$, only superharmonics with $n \lesssim 3$ grow to significant amplitude, as expected from the small value of $\alpha/\epsilon \simeq 0.26$. These grow and decay in amplitude with the predicted beat period $2\pi/(\epsilon\omega) \simeq 7700/N_0$. The parent wave amplitude barely deviates from its initial value in this case. In all the other cases considered, successive superharmonics are excited, with these growing to significant amplitude while the parent wave amplitude decreases substantially. Notably, the cascade is not monotonic with energy progressively passing to higher superharmonics. Particularly in cases with $f = 0$, high-order superharmonics rapidly grow to amplitudes larger than a_2, but the $2k$-superharmonic can then dominate once more (for example, at time $N_0t \simeq 40\,000$ if $\alpha = 0.025$, as shown in figure 3(d), and at time $N_0t \simeq 23\,000$ if $\alpha = 0.075$, as shown in figure 3e).

It may seem that the competing superharmonics would manifest as a form of wave turbulence. However, as shown below, the superposition of superharmonics in cases with $\alpha/\epsilon \gtrsim 1$ results in the manifestation of a coherent, though not steady, solitary wave train. Finally, we note that the truncated system of equations leads to an energy conservation relation, at least for $n_\star \leq 3$. As shown in Appendix B, even as superharmonics grow at the expense of the parent wave, the sum of the squared amplitudes of all the waves remains close to $|a_1(T = 0)|^2 = 1$.

4. Fully nonlinear solutions

For the purposes of testing the above prediction for the evolution of the internal tide, we performed fully nonlinear numerical simulations and ran diagnostics to compare the evolution of the primary wave amplitude and the amplitudes of each superharmonic.

The fully nonlinear equations were solved using the code described in detail in Sutherland (2016). The two-dimensional rotating Boussinesq equations were solved in a rectangular domain with horizontally periodic boundary conditions, and free-slip conditions at the top and bottom of the domain. Explicitly, the code solved the time evolution equations for spanwise vorticity (ζ), spanwise velocity (v), and the buoyancy b:

$$\zeta_t = -u\zeta_x - w\zeta_z - b_x + fv_z + Re^{-1}\mathcal{D}\zeta, \tag{4.1}$$

$$v_t = -uv_x - wv_z - fu + Re^{-1}\mathcal{D}v, \tag{4.2}$$

$$b_t = -ub_x - wb_z - N^2b + Re\,Pr^{-1}\mathcal{D}b, \tag{4.3}$$

which are extensions, respectively, of (3.4), (3.1b) and (3.2) to include viscous and diffusive terms. The fields were discretized vertically on an evenly spaced grid, and horizontally in terms of their horizontal Fourier components. The diffusion operator $\mathcal{D}$ is a Laplacian operator acting only upon horizontal Fourier components with horizontal wavenumbers greater than $32k$, in which k is the prescribed horizontal wavenumber of the parent wave. The Reynolds number $Re = H^2N_0/\nu$ was set to 10^5, and the Prandtl number Pr was set to 1. Although these values are smaller than realistic oceanographic values, they serve to damp numerical noise. Because no diffusivity was applied to disturbances with wavenumbers smaller than $32k$, the parent wave and superharmonics that grow to

significant amplitude were not attenuated. At any time, the streamfunction was found by solving $\zeta = -\nabla^2 \psi$ and, from this, u and w were found using (3.3a,b).

The background squared buoyancy frequency in all simulations presented here was exponential, given by (3.10) with $d/H = 0.04$ and $z_0 = -0.019H$. The code worked in non-dimensional variables, with length and time scales set effectively by prescribing $H = 1$ and $N_0 = 1$. However, for clarity, all variables below are given in units of H and N_0.

In the simulations presented here, the horizontal wavenumber was prescribed by $kH = 0.2$, and the Coriolis parameter was given by either $f = 0.003N_0$ or $f = 0$. For given k and f, the vertical structure of the primary wave and its frequency was found by using a Galerkin method to solve (3.9), extracting the lowest frequency solution that corresponds to a mode-1 wave. The polarization relations were then used to initialize the code with the corresponding spanwise vorticity, spanwise velocity and buoyancy fields for one wavelength of the parent wave. In the simulations presented here the maximum vertical displacement amplitude, A_0, was set to be $A_0 = 0.001H$, $0.003H$ and $0.005H$, corresponding to $\alpha = 0.025$, 0.075 and 0.125, respectively.

We begin by examining the evolution of a relatively small amplitude internal tide with $A_0 = 0.001H$ in background rotation representative of that near Hawaii, for which $f = 0.003N_0$ (for dimensional units, see § 2). For the primary wave with $kH = 0.2$, its frequency is $\omega \simeq 0.0085N_0$, and from the frequency of the $2k$-superharmonic, we have $\epsilon = 0.096$. Because $\alpha/\epsilon \sim 0.26$ is somewhat smaller than 1, only the lowest superharmonics are expected to grow to significant amplitude, and they are anticipated to beat with a period $2\pi/(\epsilon\omega) \simeq 7.7 \times 10^3/N_0$. With $N_0 = 0.017 \text{ s}^{-1}$, this corresponds to a time of 5.2 days.

The results of the simulation and comparisons with theory are shown in figure 4. Here we choose to represent the results in terms of the horizontal velocity. A snapshot of the total horizontal velocity is shown at time $N_0 t = 4000$, corresponding to 2.7 days (figure 4a). This time is approximately half the predicted beat period of the superharmonics. To reveal more clearly the superharmonics, figure 4(b) plots the horizontal velocity field after subtracting the signal from the primary wave. The snapshots show that the horizontally periodic structure of the parent wave is slightly modulated by the growth of superharmonics. At the surface, the positive (waveward) flow of the total horizontal velocity (figure 4a) extends over a shorter horizontal extent than the negative flow, and it is larger in magnitude than the negative flow. Primarily, this is a consequence of the positive flow of the $2k$-superharmonic interfering constructively with the positive flow of the parent wave, and interfering destructively with its negative flow.

By Fourier decomposing the horizontal flow at the surface at each time, we compare the time evolutions of the simulated amplitude of the primary wave and its superharmonics with those predicted by theory. Explicitly, from the predicted amplitudes, $a_n(T) = a_n(\epsilon t)$, the magnitude of the surface flow associated with disturbances of horizontal wavenumber nk is $\|u_n\| = \alpha(\omega d/k) |\hat{\psi}'(0)| a_n$. Figure 4($c$) shows excellent agreement between the simulated and predicted amplitudes of the primary wave and its first two superharmonics. Unlike the theory, the simulations exhibited small-scale oscillations about the predicted parent wave amplitude. These were due predominantly to weak interactions between the parent wave and the induced Eulerian flow, which has a mixed mode-1/mode-2 structure (Sutherland & Yassin 2022). The results show that for the moderately small value of α/ϵ in this simulation, only the $2k$- and $3k$-superharmonics grow to significant amplitude, and the amplitude of the parent wave decreases only slightly by the time the superharmonics have grown to their largest amplitude at $N_0 t \simeq 4000$.
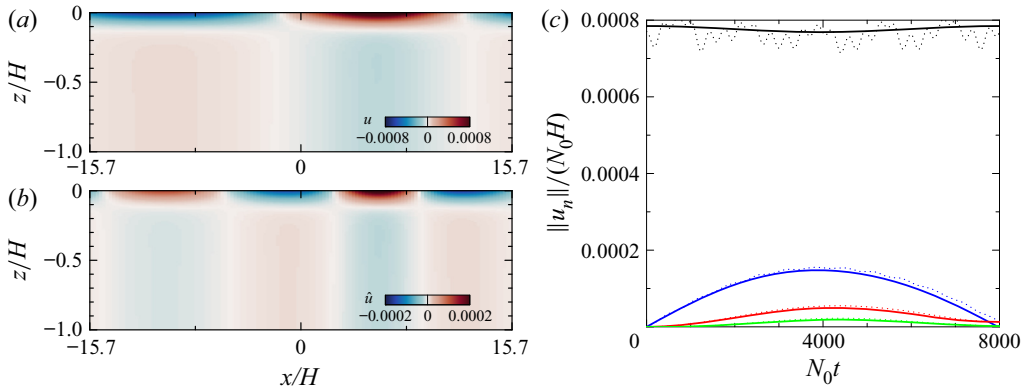
Figure 4. Supplementary movies are available at https://doi.org/10.1017/jfm.2022.689. From a simulation with $f = 0.003N_0$ and $A_0 = 0.001H$ ($\alpha = 0.025$), snapshots at $N_0 t = 4000$ of (*a*) the total horizontal velocity field and (*b*) the horizontal velocity field with the parent wave removed. (*c*) The simulated (dotted lines) and predicted (solid lines) peak horizontal velocity at $z = 0$ associated with the parent wave (black) and superharmonics with $n = 2$ (blue), $n = 3$ (red) and $n = 4$ (green). In all cases, $kH = 0.2$ and the background stratification is exponential with $N = N_0$ at $z_0 = -0.019H$ and $d = 0.04H$.

By increasing the parent wave amplitude or by considering the wave evolution at lower latitudes, hence smaller f and larger ϵ, higher superharmonics grow to significant amplitude and the parent wave amplitude decreases non-negligibly. This is shown in the results of five simulations plotted in figure 5. Here, only the total horizontal velocity field is shown in the left-hand snapshots. The right-hand plots show the time evolution of the peak horizontal velocity at $z = 0$ for the parent wave and for the $2k$-, $3k$- and $4k$-superharmonics. Higher superharmonics also grow to significant amplitude, but these are not plotted. Focusing on the right-hand plots, we see that the prediction of theory agrees well with the results of numerical simulations. For $\alpha/\epsilon \gtrsim 1$, a superharmonic cascade becomes more evident with higher superharmonics being excited and the parent wave amplitude decreasing significantly. In the cases with $f = 0$, $\omega \simeq 0.0080$ and $\epsilon \simeq 0.0035$, the predicted beat period resulting from interactions between the parent wave and the $2k$-superharmonic alone is $2\pi/(\epsilon\omega) \simeq 2 \times 10^5/N_0$ (equivalent to $\simeq 136$ days). Although the range of times examined in figures 5(*c*–*e*) is much smaller than the beat period, the superharmonics are observed to grow to substantial amplitude owing to the large values of α/ϵ.

In all cases with $\alpha/\epsilon \gtrsim 1$, the superposition of superharmonics upon the parent wave eventually results in the formation of a solitary wave train. This is characterized by a sequence of localized disturbances with enhanced positive flow near the surface. As shown in the next section, each localized disturbance is associated with a wave of depression, where the isopycnal displacement has maximum downward extent. More waves in the wave train occur and develop more rapidly if α/ϵ is larger. Thus although multiple superharmonics are excited, their phase relationship results in a coherent wave pattern rather than devolving into a random wave field. Such patterns have also been produced through separate models based upon extensions of shallow-water theory. The comparison between our theory and the shallow-water models is presented next.

5. Comparison with shallow-water theory

Several studies have examined the nonlinear evolution of the internal tide through extensions of shallow-water theory. Here, we compare the predictions of our model with
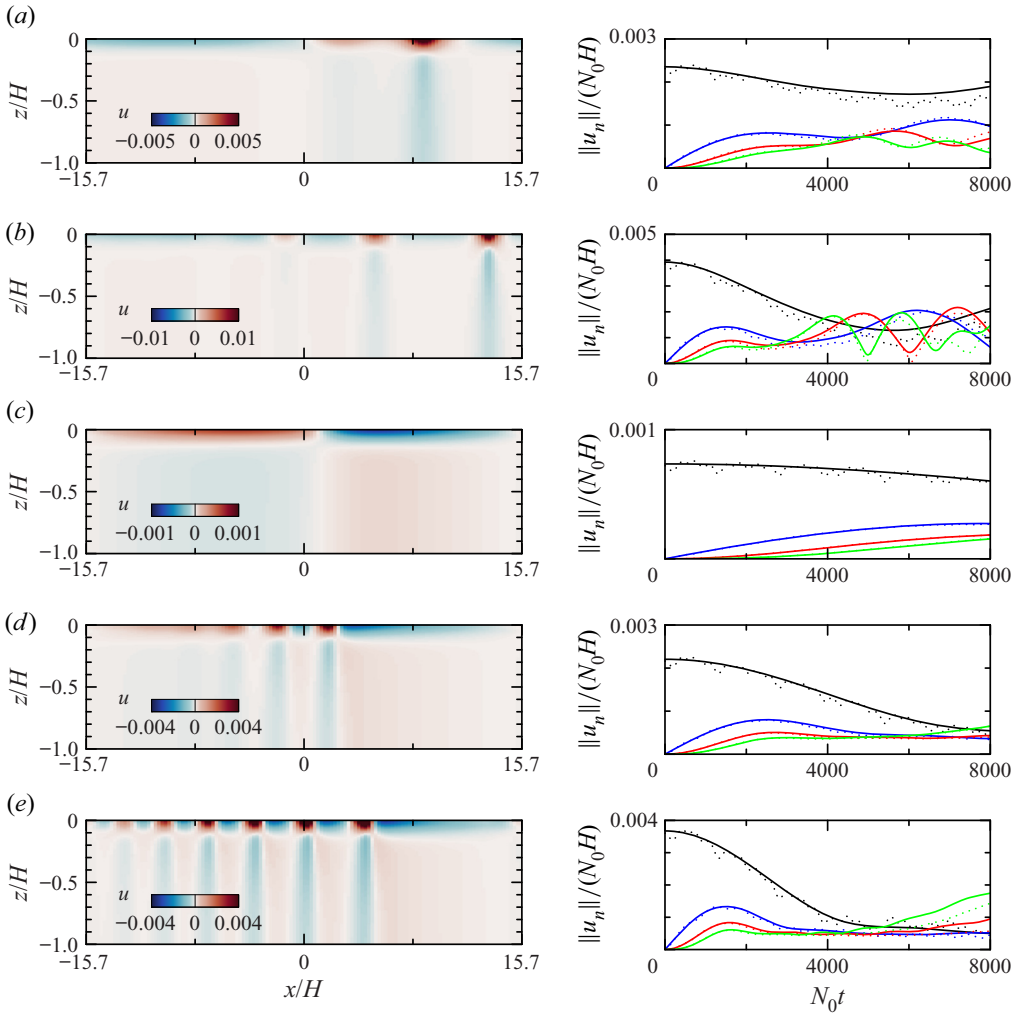
Figure 5. (There are supplementary movies for (*b*,*e*).) As in figures 4(*a*,*b*), showing (left) snapshots of the total horizontal velocity field at $N_0 t = 4000$ and (right) the simulated (dotted) and predicted (solid) time evolutions of the peak surface horizontal velocity for the parent and first three superharmonics for five different cases, with: (*a*) $f = 0.003N_0$, $A_0 = 0.003H$, $\alpha/\epsilon \simeq 0.78$; (*b*) $f = 0.003N_0$, $A_0 = 0.005H$, $\alpha/\epsilon \simeq 1.30$; (*c*) $f = 0$, $A_0 = 0.001H$, $\alpha/\epsilon \simeq 7.1$; (*d*) $f = 0$, $A_0 = 0.003H$, $\alpha/\epsilon \simeq 21$; and (*e*) $f = 0$, $A_0 = 0.005H$, $\alpha/\epsilon \simeq 36$.

two models, namely the Ostrovsky (hereafter KdV-f) equation (Ostrovsky & Stepanyants 1989) and the Miyata–Choi–Camassa equations (Miyata 1988; Choi & Camassa 1999), adapted to include the influence of rotation (Helfrich & Grimshaw 2008). The latter model we refer to hereafter as the MCC-f equations.

The KdV-f equation is an extension of the Korteweg–de Vries (KdV) equation that includes the influence of background rotation. Following the notation used above, it is assumed that the vertical displacement field associated with the waves is separable, so $\xi(x, z, t) = \eta(x, t)\,\hat{\psi}(z)$, in which η satisfies (Ostrovsky & Stepanyants 1989)

$$\frac{\partial}{\partial x}\left[\frac{\partial \eta}{\partial t} + c_0\,\frac{\partial \eta}{\partial x} + \alpha_k \eta\,\frac{\partial \eta}{\partial x} + \beta_k\,\frac{\partial^3 \eta}{\partial x^3}\right] = \frac{f^2}{2c_0}\,\eta. \tag{5.1}$$

Here, c_0 is the long-wave speed found in a system with zero background rotation, and α_k and β_k are parameters respectively representing the importance of nonlinearity and non-hydrostatic effects. These are determined explicitly in terms of the vertical structure function $\hat{\psi}$ (Benney 1966; Grimshaw & Helfrich 2012). Explicitly, in the Boussinesq approximation, we have

$$\alpha_k = \frac{3}{2} c_0 \frac{\displaystyle\int (\hat{\psi}')^3 \, \mathrm{d}z}{\displaystyle\int (\hat{\psi}')^2 \, \mathrm{d}z}, \quad \beta_k = \frac{1}{2} c_0 \frac{\displaystyle\int \hat{\psi}^2 \, \mathrm{d}z}{\displaystyle\int (\hat{\psi}')^2 \, \mathrm{d}z}. \tag{5.2a,b}$$

Given that the scale of η is $A_0 = \alpha d$, the scale of the nonlinear term relative to the advection term is $d\alpha\alpha_k/c_0 \sim \alpha$, and the scale of the non-hydrostatic term relative to the advection term is $\beta_k k^2/c_0 \sim d^2 k^2$. In these approximations, it is assumed that $\hat{\psi}'$ scales as $1/d$, the inverse characteristic depth of the stratification. The scale of the term representing the influence of rotation relative to advection is $f^2/(c_0 k)^2 \sim (f/\omega)^2$. The approximations leading to (5.1) assume that these three scales are in balance and small: $\alpha \sim (dk)^2 \sim (f/\omega)^2 \ll 1$.

The MCC-f equations have been formulated for a two-layer system, in which the upper layer has depth h_1, and the density jump between the lower and upper layer is represented by the reduced gravity g'. The coupled equations are cast in terms of the upper-layer depth in the presence of an interfacial wave, $h = h_1 - \eta$, the horizontal velocity differences between the lower and upper layers in the along-wave direction, $U = u_2 - u_1$, and across-wave direction, $V = v_2 - v_1$, and in terms of the barotropic transport in the across-wave direction, $Q = v_1 h + v_2(H - h)$. The barotropic transport in the along-wave direction is assumed to be zero: $u_1 h + u_2(H - h) = 0$. Explicitly, the MCC-f equations are (Helfrich & Grimshaw 2008)

$$\frac{\partial h}{\partial t} = \frac{\partial}{\partial x}\left[Uh\left(1 - \frac{h}{H}\right)\right], \tag{5.3}$$

$$\frac{\partial U}{\partial t} = \frac{\partial}{\partial x}\left[\frac{1}{2} U^2 \left(1 - 2\frac{h}{H}\right) + g'h\right] + fV + (D_2 - D_1), \tag{5.4}$$

$$\frac{\partial V}{\partial t} = -U\left[V\frac{1}{H}\frac{\partial h}{\partial x} - \frac{\partial V}{\partial x}\left(1 - 2\frac{h}{H}\right) + \frac{\partial Q}{\partial x} + f\right], \tag{5.5}$$

$$\frac{\partial Q}{\partial t} = -\frac{\partial}{\partial x}\left[UVh\left(1 - \frac{h}{H}\right)\right]. \tag{5.6}$$

Here, the non-hydrostatic terms are represented by D_1 and D_2:

$$D_i = \frac{1}{h_i}\frac{\partial}{\partial x}\left[\frac{1}{3} h_i^3 \left(\frac{\partial^2 u_i}{\partial x \, \partial t} + u_i \frac{\partial^2 u_i}{\partial x^2} - \left(\frac{\partial u_i}{\partial x}\right)^2 \right)\right], \quad i = 1, 2, \tag{5.7}$$

in which $h_2 = H - h_1$.

In order to compare our model results, for which the background stratification is continuous, to this two-layer model, we use (5.2a,b), in which the vertical structure

function is that for a two-layer stratification. Thus we find

$$c_0 = \sqrt{g'\bar{H}}, \quad \alpha_k = -\frac{3}{2} c_0 \frac{1}{\bar{H}} \left(1 - 2\frac{h_1}{H_{2L}}\right), \quad \beta_k = \frac{1}{6} c_0 H_{2L}\bar{H}, \quad (5.8a\text{--}c)$$

in which $\bar{H} = h_1(H_{2L} - h_1)/H_{2L}$, and H_{2L} is the total equivalent depth. These equations can be inverted so that, for given c_0, α_k and β_k (determined from a system with continuous stratification), we determine the equivalent total depth and upper-layer depth, given respectively by

$$H_{2L} = 4\frac{\alpha_k\beta_k}{c_0^2}\left[1 + \sqrt{1 + \frac{3c_0^3}{2\alpha_k^2\beta_k}}\right], \quad (5.9)$$

$$h_1 = 2\frac{\alpha_k\beta_k}{c_0^2} + H_{2L}/2. \quad (5.10)$$

For proper comparison with our theory and the KdV-f equation, the equivalent reduced gravity should be defined based upon the shallow-water speed c_f, determined from the dispersion relation that includes the influence of background rotation. Explicitly, $c_f = (\omega^2 - f^2)^{1/2}/k$ and $g' = c_f^2/\bar{H}$.

We solved the KdV-f equation by Fourier transforming η in x, and then time-evolving the Fourier amplitudes. The MCC-f model was discretized in space with x-derivatives approximated by centred second-order finite differences. Both models were advanced in time using a fourth-order Adams–Bashforth–Moulton predictor–corrector scheme. The corrector step was iterated until the magnitude of the relative difference between successive fields was less than a tolerance of 10^{-6}. These equations were solved in MATLAB. Integrating in time up to $N_0 t = 5000$ was accomplished in seconds using our equations, in minutes for the KdV-f equation, and in about an hour for the MCC-f equations.

We compare the predictions of our theory with the KdV-f and MCC-f predictions for the two cases considered in figures 5(*a,d*), for which $A_0 = 0.003H$, and $f = 0.003N_0$ and $f = 0$. For the exponential stratification prescribed for those cases, the corresponding vertical structure functions give the coefficients of the KdV-f equation to be $c_0 \simeq 0.040N_0H$, $\alpha_k \simeq -0.80N_0$, $\beta_k \simeq 0.00060N_0H^3$ and $f^2/(2c_0) \simeq 0.00011N_0$ in the case $f = 0.003N_0$. The equivalent parameters for the two-layer system of the MCC-f equations are $H_{2L} \simeq 1.31H$, $h_1 \simeq 0.073H$ and $g' \simeq 0.023N_0^2H$.

The predictions of the three models are shown in figure 6. For both cases with $f = 0.003N_0$ and $f = 0$, there is good qualitative agreement between the three models. All show the emergence of a single localized wave of depression in the case with $f = 0.003N_0$, and a solitary wave train in the case with $f = 0$. Quantitatively, the MCC-f model gives the poorest agreement, predicting that the waves are narrower with more waves in the wave train.

Despite these minor discrepancies, it is reassuring that our superharmonic cascade model reproduces the results of the well-established shallow-water models when the parameters governing the amplitude and the importance of non-hydrostatic effects are in the appropriate regime.

6. Conclusion

We have extended the model of Baker & Sutherland (2020) to include resonances between a vertical mode-1 internal tide and an arbitrary number of its mode-1 superharmonics.
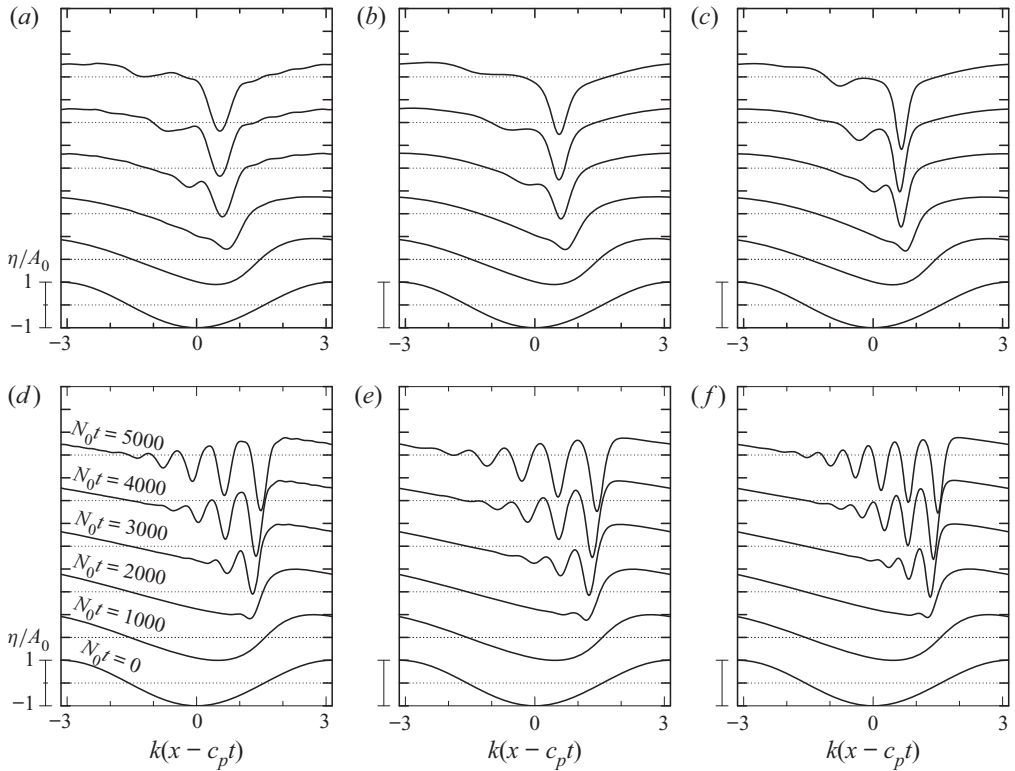
Figure 6. Comparison of vertical displacement predicted by (*a*,*d*) the superharmonic cascade (SHC) model, (*b*,*e*) the KdV-f equation, and (*c*,*f*) the MCC-f model, in cases with $kH = 0.2$, $A_0 = 0.003$ and (*a*–*c*) $f = 0.003N_0$, and (*d*–*f*) $f = 0$. For SHC and KdV-f, the background stratification is exponential with $N = N_0$ at $z_0 = -0.019H$ and $d = 0.04H$. For MCC-f, the equivalent parameters of the two-layer system are computed from the corresponding coefficients computed for the KdV-f equation. In all cases, the displacement is plotted at evenly spaced times, as indicated in (*d*), with successive times being vertically offset. The plots are given in a frame of reference moving with the phase speed c_p of the parent wave.

The key parameter determining how many superharmonics contribute to the nonlinear evolution of the tide is given by α/ϵ, which measures the relative amplitude of the parent wave to the relative beat frequency of the parent wave and its $2k$-superharmonic. If $\alpha/\epsilon \gtrsim 0.1$, then superharmonics greater than $2k$ play a non-negligible role in the evolution of the tide. A periodic growth and decay of low superharmonics occurs if $\alpha/\epsilon \lesssim 1$. For larger α/ϵ, a superharmonic cascade occurs, resulting in the internal tide transforming into a internal solitary wave train. The structure of this wave train is consistent with the predictions of well-established shallow models, KdV-f and MCC-f, that include weak non-hydrostatic effects and the influence of rotation.

Our model provides new physical insight into the processes leading to internal solitary wave trains. Generally, with the main assumption being that the parent wave and all superharmonics have a vertical mode-1 structure, the system of coupled ordinary differential equations predicts the fully nonlinear evolution of the internal tide with no restrictions on the degree to which the initial wave is non-hydrostatic (through the parameter $\beta_k k^2/c_0 \sim (kd)^2$), large-amplitude (through the parameter $\alpha = A_0 k$) or influenced by rotation (through the parameter $f^2/(c_0 k)^2 \sim (f/\omega)^2$). The solution of the coupled equations agrees very well with the results of fully nonlinear numerical

948 A21-18

simulations, demonstrating that it is reasonable to restrict superharmonic disturbances to have vertical mode-1 structure. Furthermore, being a system of coupled ordinary differential equations, not involving spatial derivatives, solutions can be found quickly on a single processor in comparison with the KdV-f and MCC-f models.

Our study was focused upon examining a parameter regime consistent with observations of the M_2 internal tide that emanates south-westward from Hawaii toward the equator. Though we could also have applied to the model to study the well-documented formation of internal solitary wave trains in the South China Sea (e.g. see Alford *et al.* 2010; Li & Farmer 2011), our interest here is in the increasing influence of nonlinear effects upon the evolution of the internal tide as it approaches the equator. Using parameters based upon observations, we predict that the internal tide near Hawaii would be only weakly perturbed by superharmonics during the neap tide, but a solitary wave would develop during the spring tide. This would develop in a time of the order of $4000/N_0 \simeq 3$ days. In that time, the tide would have propagated at the group velocity $c_g \simeq 0.037HN_0 \simeq 3.3$ m s^{-1}, a distance of $\simeq 780$ km. This distance is sufficiently small to justify the approximation used in theory and simulations to predict the emergence of solitary waves on the f-plane.

Of course, other than the assumption that the disturbances have a mode-1 vertical structure, there are several other simplifying assumptions of the model: it is restricted to two dimensions (being spanwise-invariant), it ignores background currents, the domain depth and Coriolis parameter are assumed to be constant, and the parent wave is periodic. Future theoretical work will relax the assumption of constant H and f using the Wentzel–Kramers–Brillouin (WKB) approximation, and the influence of the finite spanwise extent of internal tide beams will also be considered. In a companion paper, we relax the assumption of periodicity of the internal tide to examine a spatially modulated internal tide both in theory and simulations (Sutherland & Yassin 2022). Therein it is shown that the self-interaction of the internal tide and its superharmonics leads to a near-steady forcing of an induced Eulerian flow whose magnitude remains sufficiently small to have negligible influence upon the evolution of the internal tide and its superharmonics.

Supplementary movies. Supplementary movies are available at https://doi.org/10.1017/jfm.2022.689.

Declaration of interests. The authors report no conflict of interest.

Author ORCIDs.
Bruce R. Sutherland https://orcid.org/0000-0002-9585-779X.

Appendix A. Long-wave approximation

In developing the theory in § 3 for the excitation of superharmonics and their interactions, the only approximation made was that the primary wave and superharmonics all had a mode-1 vertical structure. No restriction was put on the frequency of the waves relative to f or N_0. Because our motivation is to examine the evolution of an internal tide, for which $kH \ll 1$ and $\omega \ll N_0$, we may further simplify the expressions for the interaction coefficients (3.22) and (3.23) as well as the slow phase-shift coefficients B_n given by (3.18*a,b*).

If $f = 0$, then the vertical structure $\bar{\psi}$ of long waves is given by the solution for mode-1 waves of the eigenvalue problem $\bar{\psi}'' = -(1/c^2)N^2\bar{\psi}$ in which the eigenvalue is

the long-wave speed c. This follows by taking $f = 0$ in (3.9) and assuming $\omega \ll N_0$. The corresponding dispersion relation is

$$\omega^2 \simeq c^2 k^2, \tag{A1}$$

for $kH \ll 1$. Putting $f = 0$ in (3.22) and using $\omega_n = c(nk)$, we find

$$E_{mm} \simeq \frac{n}{4} d \left[\int_{-H}^{0} N^2 \bar{\psi}^2 \, dz \right]^{-1} \left[\int_{-H}^{0} \frac{dN^2}{dz} \bar{\psi}^3 \, dz \right], \tag{A2}$$

in which $n = 2m$. Similarly for $m > l$, using the approximate dispersion relation in (3.23) and using $n = m + l$, we find

$$E_{ml} \simeq \frac{n}{2} d \left[\int_{-H}^{0} N^2 \bar{\psi}^2 \, dz \right]^{-1} \left[\int_{-H}^{0} \frac{dN^2}{dz} \bar{\psi}^3 \, dz \right]. \tag{A3}$$

This is just twice the value of E_{mm} for the same value of n.

If $|f| > 0$, then the vertical structure of long waves satisfies $\bar{\psi}'' = -\kappa^2 (N^2/f^2 - 1)\bar{\psi}$, and the dispersion relation is

$$\omega^2 \simeq f^2 (1 + k^2/\kappa^2), \tag{A4}$$

in which κ is the eigenvalue. We can then simplify (3.22) by writing $\omega_n^2 - f^2 \simeq f^2 (nk)^2/\kappa^2$. If we further assume $\|N\| \gg f$, then the self-interaction coupling coefficients simplify to

$$E_{mm} \simeq \frac{n}{4} d \frac{1}{1 + k^2/\kappa^2} \left[\int_{-H}^{0} N^2 \bar{\psi}^2 \, dz \right]^{-1} \left\{ \left(\frac{k^2}{\kappa^2} + \frac{n^2 + 2}{2n^2} \right) \left[\int_{-H}^{0} \frac{dN^2}{dz} \bar{\psi}^3 \, dz \right] \right\}. \tag{A5}$$

To estimate the E_{ml} interaction coefficients, we further assume that $\omega_n \ll N_0$ for the nk-superharmonics of interest. Hence we can write $(N^2 - \omega_n^2)/(\omega_n^2 - f^2) \simeq (N^2/f^2)(nk)^2/\kappa^2$. The expression in (3.23) thus simplifies to

$$E_{ml} \simeq \frac{n}{2} d \frac{1}{1 + k^2/\kappa^2} \left[\int_{-H}^{0} N^2 \bar{\psi}^2 \, dz \right]^{-1} \left\{ \left(\frac{k^2}{\kappa^2} + \frac{n^2 ml + m^2 + l^2}{2n^2 ml} \right) \left[\int_{-H}^{0} \frac{dN^2}{dz} \bar{\psi}^3 \, dz \right] \right\}. \tag{A6}$$

For the exponential stratification given by (3.10) with $d = 0.04H$ and $z_0 = -0.019H$, the empirical solution of the eigenvalue problem gives $\kappa H \simeq 25 f/N_0$ for $f \lesssim 0.003 N_0$. Hence at these low latitudes, $(k/\kappa)^2 \simeq 7.1 \gg 1$ for a primary wave with $kH = 0.2$. This allows us to approximate further (A5) and (A6), resulting in the expressions found for $f = 0$ given respectively by (A2) and (A3).

In the case with $|f| > 0$, we can use the dispersion relation (A4) to find approximate expressions for the time phase-shift coefficients B_n in (3.18a,b). Explicitly,

$$B_n \simeq \frac{2}{3} \frac{n+1}{n}, \quad n = 2, 3, \ldots. \tag{A7}$$

This decreases from 1 to $2/3$ as n increases from 2.

948 A21-20

Appendix B. Energy conservation

As shown by Baker & Sutherland (2020), the coupled pair of equations given by (3.24a,b) leads to an energy conservation relation

$$|a_1|^2 + \frac{E_{2,-1}}{E_{1,1}} |a_2|^2 = \text{const.} \tag{B1}$$

Similarly, the system of equations truncated at $n_\star = 3$ leads to the following conservation law:

$$|a_1|^2 + \frac{E_{2,-1}}{E_{1,1}} |a_2|^2 + \left(\frac{E_{3,-2}}{E_{2,1}} + \frac{E_{3,-1}}{E_{2,1}} \frac{E_{2,-1}}{E_{1,1}} \right) |a_3|^2 = \text{const.} \tag{B2}$$

These relations may be simplified further using the approximate formulae for the interaction coefficients given by (A2) and (A3). The integrals in these expressions cancel upon taking the ratio of the interaction coefficients, so that

$$\frac{E_{ml}}{E_{pq}} \simeq \begin{cases} (m+l)/(p+q) & m \neq l, p \neq q, \\ (m+l)/p & m \neq l, p = q. \end{cases} \tag{B3}$$

In particular, $E_{2,-1}/E_{1,1} \simeq 1$, $E_{3,-2}/E_{2,1} \simeq 1/3$ and $E_{3,-1}/E_{2,1} \simeq 2/3$. Hence in (B1) and (B2), we have, respectively, $|a_1|^2 + |a_2|^2 \simeq 1$ and $|a_1|^2 + |a_2|^2 + |a_3|^2 \simeq 1$, in which we have used the initial conditions $a_1(0) = 1$ and $a_n(0) = 0$ for $n \geq 2$.

REFERENCES

ALFORD, M.H. 2003 Redistribution of energy available for ocean mixing by long-range propagation of internal waves. *Nature* **423**, 159–162.

ALFORD, M.H., LIEN, R.-C., SIMMONS, H., KLYMAK, J.M., RAMP, S., YANG, Y.J., TANG, D. & CHANG, M.-H. 2010 Speed and evolution of nonlinear internal waves transiting the South China Sea. *J. Phys. Oceanogr.* **40**, 1338–1355.

ALFORD, M.H., MACKINNON, J.A., ZHAO, Z., PINKEL, R., KLYMAK, J. & PEACOCK, T. 2007 Internal waves across the Pacific. *Geophys. Res. Lett.* **34**, L24601.

BAKER, L. & SUTHERLAND, B.R. 2020 The evolution of superharmonics excited by internal tides in non-uniform stratification. *J. Fluid Mech.* **891**, R1.

BALMFORTH, N.J., IERLEY, G.R. & YOUNG, W.R. 2002 Tidal conversion by subcritical topography. *J. Phys. Oceanogr.* **32** (10), 2900–2914.

BENNEY, D.J. 1966 Long nonlinear waves in fluid flows. *J. Math. Phys.* **45**, 52–63.

VAN DEN BREMER, T.S., YASSIN, H. & SUTHERLAND, B.R. 2019 Lagrangian transport by vertically confined internal gravity wavepackets. *J. Fluid Mech.* **864**, 348–380.

BÜHLER, O. 2014 *Waves and Mean Flows*, 2nd edn. Cambridge University Press.

CHOI, W. & CAMASSA, R. 1999 Fully nonlinear internal waves in a two-fluid system. *J. Fluid Mech.* **396**, 1–36.

DIAMESSIS, P.J., WUNSCH, S., DELWICHE, I. & RICHTER, M.P. 2014 Nonlinear generation of harmonics through the interaction of an internal wave beam with a model oceanic pycnocline. *Dyn. Atmos. Oceans* **66**, 110–137.

GRIMSHAW, R.H.J. & HELFRICH, K.R. 2012 The effect of rotation on internal solitary waves. *IMA J. Appl. Maths* **77**, 326–339.

GRISOUARD, N., STAQUET, C. & GERKEMA, T. 2011 Generation of internal solitary waves in a pycnocline by an internal wave beam: a numerical study. *J. Fluid Mech.* **676**, 491–513.

HELFRICH, K.R. & GRIMSHAW, R.H.J. 2008 Nonlinear disintegration of the internal tide. *J. Phys. Oceanogr.* **38**, 686–701.

KLYMAK, J.M., SIMMONS, H.L., BRAZNIKOV, D., KELLY, S., MACKINNON, J.A., ALFORD, M.H., PINKEL, R. & NASH, J.D. 2016 Reflection of linear internal tides from realistic topography: the Tasman continental slope. *J. Phys. Oceanogr.* **46**, 3321–3337.

LEGG, S. & ADCROFT, A. 2003 Internal wave breaking at concave and convex continental slopes. *J. Phys. Oceanogr.* **33**, 2224–2246.

LI, Q. & FARMER, D.M. 2011 The generation and evolution of nonlinear internal waves in the deep basin of the South China Sea. *J. Phys. Oceanogr.* **41**, 1345–1363.

MACKINNON, J.A., ALFORD, M.H., SUN, O., PINKEL, R., ZHAO, Z. & KLYMAK, J. 2013 Parametric subharmonic instability of the internal tide at 29°N. *J. Phys. Oceanogr.* **43**, 17–28.

MACKINNON, J.A., *et al.* 2017 Climate process team on internal wave-driven ocean mixing. *Bull. Am. Meteorol. Soc.* **98**, 2429–2454.

MIYATA, M. 1988 Long internal waves of large amplitude. In *Nonlinear Water Waves* (ed. K. Horikawa & H. Maruo), pp. 399–406. Springer-Verlag.

NEW, A.L. & PINGREE, R.D. 1990 Large-amplitude internal soliton packets in the central Bay of Biscay. *Deep Sea Res.* **37** (3), 513–524.

NEW, A.L. & PINGREE, R.D. 1992 Local generation of internal soliton packets in the central Bay of Biscay. *Deep Sea Res.* **39** (9), 1521–1534.

OSTROVSKY, L.A. & STEPANYANTS, Y.. A. 1989 Do internal solitons exist in the ocean? *Rev. Geophys.* **27**, 293–310.

RAINVILLE, L., JOHNSTON, T.M.S., CARTER, G.S., MERRIFIELD, M.A., PINKEL, R., WORCESTER, P.F. & DUSHAW, B.D. 2010 Interference pattern and propagation of the M_2 internal tide south of the Hawaiian Ridge. *J. Phys. Oceanogr.* **40**, 311–325.

RAINVILLE, L. & PINKEL, R. 2006 Baroclinic energy flux at the Hawaiian Ridge: observations from the R/P FLIP. *J. Phys. Oceanogr.* **36**, 1104–1122.

SUTHERLAND, B.R. 2016 Excitation of superharmonics by internal modes in non-uniformly stratified fluid. *J. Fluid Mech.* **793**, 335–352.

SUTHERLAND, B.R. & YASSIN, H. 2022 The nonlinear evolution of internal tides. Part 2: Lagrangian transport by periodic and modulated waves. *J. Fluid Mech.* **948**, A22.

VARMA, D. & MATHUR, M. 2017 Internal wave resonant triads in finite-depth non-uniform stratifications. *J. Fluid Mech.* **824**, 286–311.

WUNSCH, S. 2015 Nonlinear harmonic generation by diurnal tides. *Dyn. Atmos. Oceans* **71**, 91–97.

WUNSCH, S. 2017 Harmonic generation by nonlinear self-interaction of a single internal wave mode. *J. Fluid Mech.* **828**, 630–647.

WUNSCH, S. & BRANDT, A. 2012 Laboratory experiments on internal wave interactions with a pycnocline. *Exp. Fluids* **53**, 1663–1679.

WUNSCH, C. & FERRARI, R. 2004 Vertical mixing, energy, and the general circulation of the oceans. *Annu. Rev. Fluid Mech.* **36**, 281–314.